Real-Time Characterization of the Organic Composition and Size of Individual Diesel Engine Smoke Particles

ARTICLE *in* ENVIRONMENTAL SCIENCE AND TECHNOLOGY · SEPTEMBER 1998

Impact Factor: 5.33 · DOI: 10.1021/es980135t

4 AUTHORS, INCLUDING:

Peter T A Reilly
Washington State University
62 PUBLICATIONS **1,115** CITATIONS

SEE PROFILE

Environ. Sci. Technol. **1998**, *32,* 2672−2679

Real-Time Characterization of the Organic Composition and Size of Individual Diesel Engine Smoke Particles

PETER T. A. REILLY,* RAINER A. GIERAY, WILLIAM B. WHITTEN, AND J. MICHAEL RAMSEY

Oak Ridge National Laboratory, P.O. Box 2008, Oak Ridge, Tennessee 37831-6142

Real-time analysis of individual diesel engine exhaust particles was demonstrated using an ion trap mass spectrometer. Measurements were made on the nebulized engine oil and diesel fuel for comparison with the exhaust particle analysis. Studies were performed on individual exhaust particles to determine composition as a function of aerodynamic size. MS/MS analysis positively identified low-mass PAHs as well as indicated the presence of high mass hydrogenated PAHs (HPAHs). The degree of PAH hydrogenation was found to be mass dependent. The origin of the HPAHs seems to be the diesel fuel. However, the HPAHs underwent some degree of oxidation during the combustion process on average. Indicators were found that might be used to determine combustion efficiency. The capability of the technique for on-line measurement of combustion processes was demonstrated.

Introduction

For many years now, exhaust emissions from gasoline and diesel powered vehicles have been studied primarily because of their adverse health effects (*1*−*5*). Yet, because of the complexity of these emissions, chemical characterization of exhaust aerosols is still ongoing (*1*). In comparison to gasoline engines, diesel engines are known to have better fuel efficiency and emit smaller amounts of volatile organic carbon (VOC) and CO_2. However, they are also known to create much larger amounts of particulate matter as well as many polycyclic aromatic hydrocarbons (PAHs). The reason for the greater diesel engine PAH emissions is due to much higher temperatures and pressures in the combustion process and to larger initial concentrations of PAHs in the diesel fuel (*4*).

The extent of human exposure to PAHs depends on partitioning between the gas and particle phases as well as the size distribution of the particulate fraction containing the PAHs, there being a much greater potential carcinogenic effect if the PAHs are components of particles that penetrate and deposit into the bronchioles and alveoli of the lungs (*6*). Moreover, some recent studies correlated health effects with the concentration of atmospheric particles, yet failed to identify the causative agents (*7, 8*). Since the toxicity of particles from different sources varies widely, such studies would be much more valuable if the particles in a distribution

* Corresponding author e-mail: reillypt@ornl.gov; phone: (423)-574-4919; fax (423)574-8363.

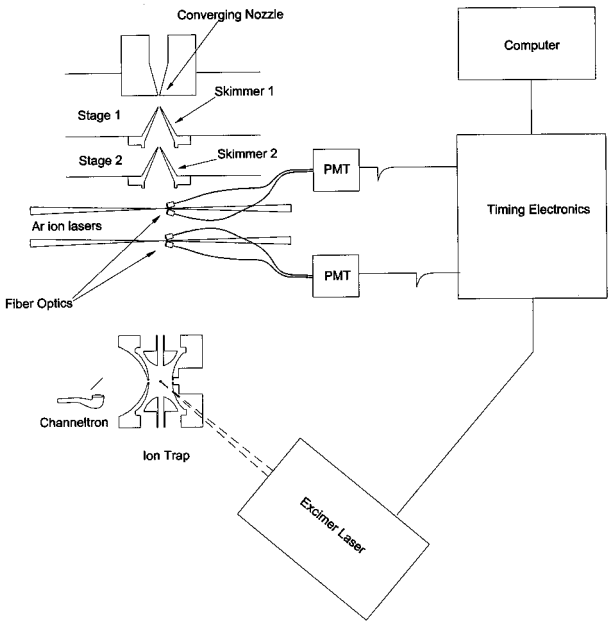

FIGURE 1. Simplified schematic diagram of the apparatus.

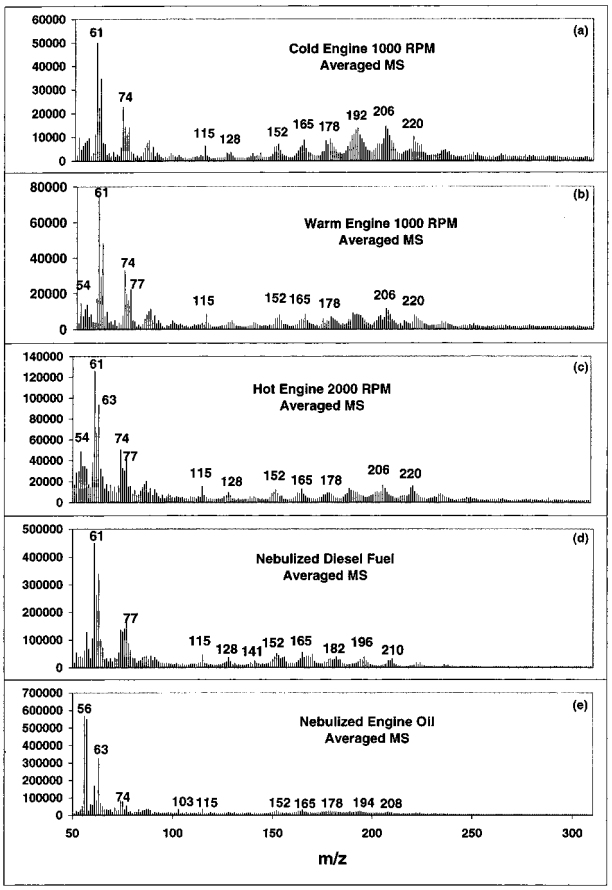

FIGURE 2. Averages from hundreds of mass spectra of individual airborne particles from (a) diesel exhaust from a cold engine idling at 1000 rpm, (b) diesel exhaust from a warm engine idling at 1000 rpm, (c) diesel exhaust from a warm engine running at 2000 rpm, (d) nebulized diesel fuel, and (e) nebulized engine oil.

S0013-936X(98)00135-7 CCC: $15.00
Published on Web 08/12/1998

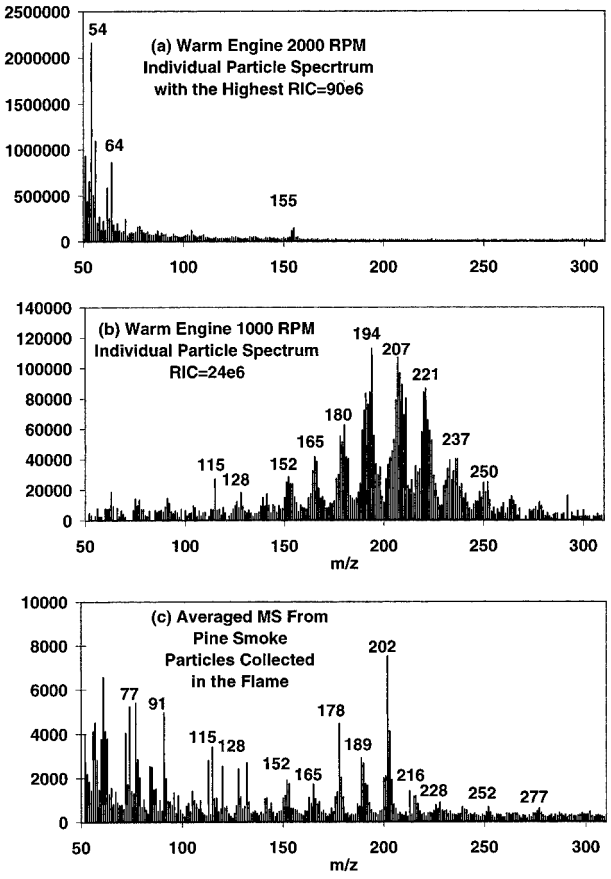

FIGURE 3. Comparison of mass spectra from (a) an individual exhaust particle from the warm engine idling at 2000 rpm that had the highest relative ion count (RIC) of any of the spectra in the survey and represents one of the extremes of composition, (b) an individual exhaust particle from the warm engine idling at 1000 rpm and represents the other extreme in exhaust particle composition, and (c) averaged mass spectrum from individual pine smoke particles collected from a flame and used as a comparison to aid identification of PAHs in the exhaust particle mass spectra.

were individually characterized with respect to size and composition rather than using bulk analysis techniques.

Real-time characterization of individual airborne particles has been reported by several groups (*9*−*16*) due to advances in laser ablation mass spectrometry. These groups have made great strides in characterizing the chemistry and composition of primarily inorganically based airborne particulate matter using a technique based on time-of-flight mass spectrometry. Characterization of organically based airborne particles, on the other hand, is a much more difficult problem because most airborne particles found in the environment are complex mixtures. Since organic compounds fragment substantially under typical mass spectral analysis, positive identification of organic species in a mixture quickly becomes challenging when more than one component is present due to matrix interference.

Recently, real-time analysis of organically based airborne particles has been demonstrated using tandem mass spectrometry in an ion trap (*17*−*20*). The ability of the ion trap to isolate and positively identify any ion in the spectrum makes it ideal for real-time analysis of organic components even in complex mixtures. In the present study, tandem mass spectrometry was used to identify some of the organic PAH components in individual diesel engine exhaust particles and to investigate the average particle composition as a function of aerodynamic particle size under various engine conditions.

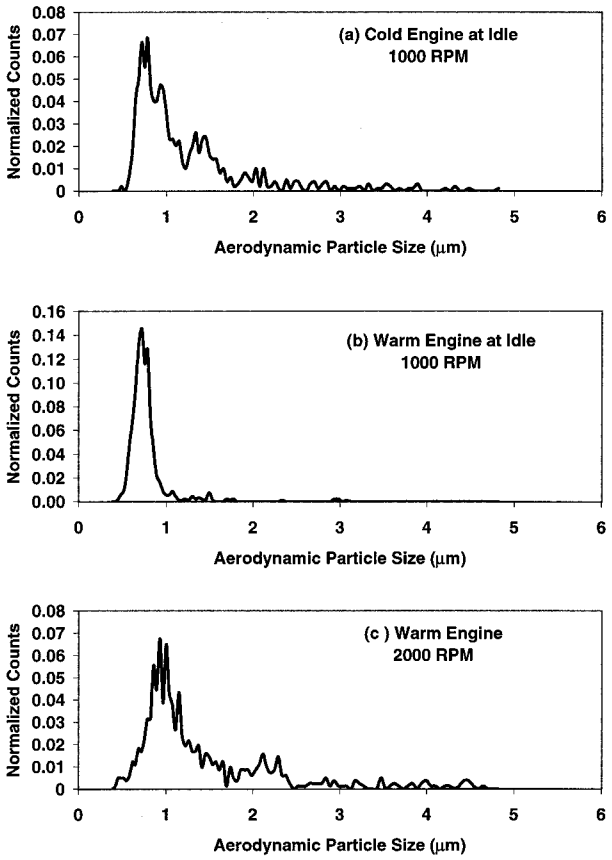

FIGURE 4. Uncorrected measured aerodynamic size distributions from the exhaust of (a) a cold diesel engine idling at 1000 rpm, (b) a warm diesel engine idling at 1000 rpm, and (c) a warm diesel engine running at 2000 rpm.

Experimental Section

The experimental apparatus was similar to that first described by Reilly et al. (*17*) and later described by Gieray et al. (*18*). A simplified schematic of the apparatus is shown in Figure 1. The differentially pumped collimating inlet system consisted of a 500 μm converging nozzle followed by 500 and 250 μm skimmers. Approximately 2.5 L of air entered the inlet system per minute. The region between the nozzle and the first skimmer was pumped with a 500 L/min roughing pump to the low Torr range. The region between the two skimmers was pumped with another 500 L/min pump to approximately 9.3 Pa.

Upon entering the main chamber, the collimated particle beam traversed two-focused Ar^+ laser beams before entering the ion trap. The laser light elastically scattered from the particles was collected by fiber optics and detected at two separate photomultiplier tubes (PMT). When the particle arrived at the center of the ion trap, a focused XeCl excimer laser was pulsed to ablate and ionize material from the particle. The nominal laser fluence was approximately 10 J/cm^2/pulse at 308 nm. A pulse of this magnitude should completely ablate a 0.5 μm particle. The ions were subsequently subjected to standard techniques for ion trap mass analysis. Approximately 47% of the detected particles yield enough ions to produce an interpretable spectrum.

The method of triggering the excimer laser to fire when the particles arrive at the exact trap center was due originally to Sinha (*9*) but has been modified to accommodate the different triggering delay of the pulsed laser (*12*, *19*). The signal from the first PMT was converted to TTL and subsequently initiated an "up-counter" chip that counted pulses from an internal 25 MHz clock. The scattered light

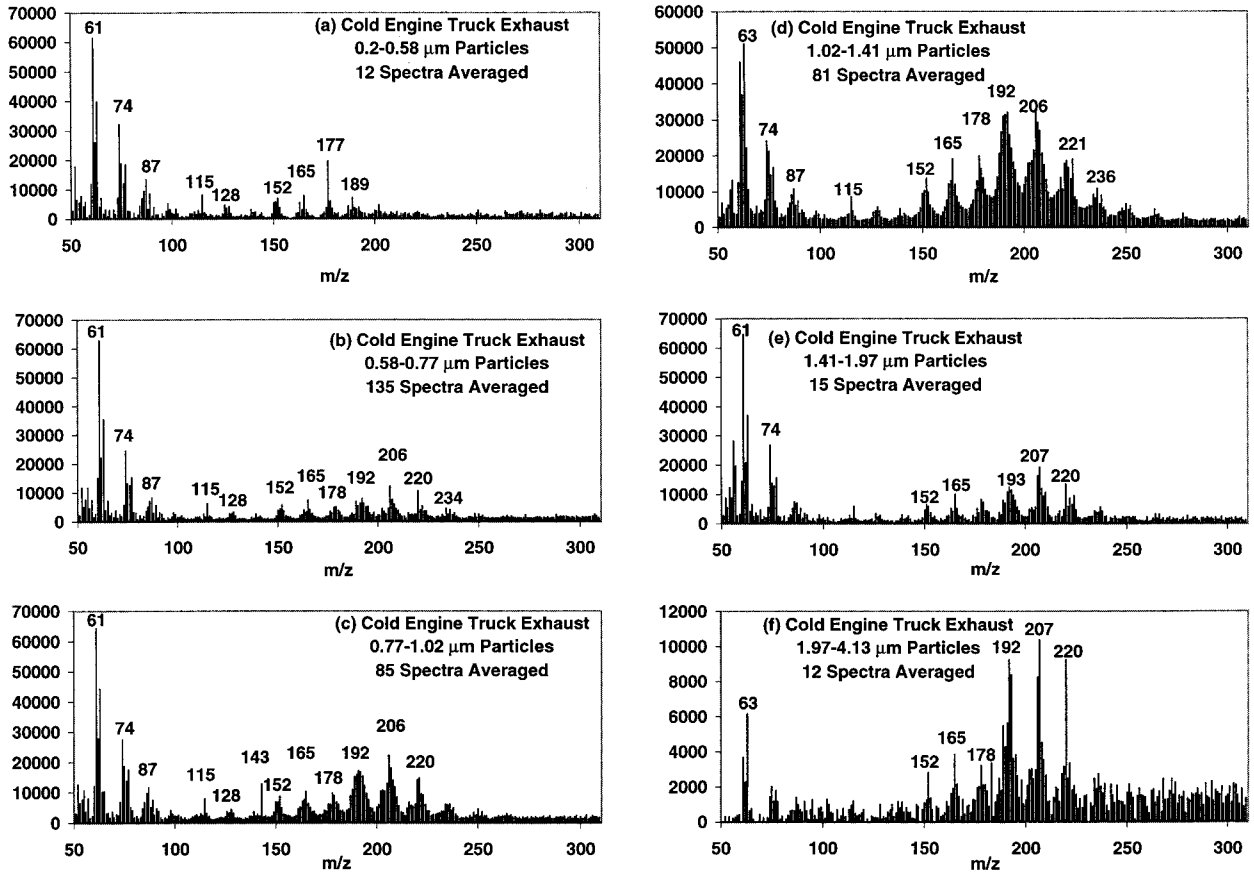

FIGURE 5. Individual exhaust particle mass spectra from a cold diesel engine idling at 1000 rpm averaged over a specified aerodynamic particle size range: (a) 0.2−0.58 μm range, 12 spectra averaged, (b) 0.58−0.77 μm range, 135 spectra averaged, (c) 0.77−1.02 μm range, 85 spectra averaged, (d) 1.02−1.41 μm range, 81 spectra averaged, (e) 1.41−1.97 μm range, 15 spectra averaged, and (f) 1.97−4.13 μm range, 12 spectra averaged.

was then detected at the second PMT and also converted to TTL. This signal stopped the "count-up" process and transferred the binary count-up number to a latch that was later recorded along with the mass spectrum. It also sent a signal to charge the excimer laser and simultaneously initiated the "down-counter" to count down from the previously counted number to zero at an externally input clock frequency. When the down-counter counted to zero, a TTL pulse was then sent to fire the laser. The external clock frequency was set so that the ratio of internal and external clock frequencies was equal to the reciprocal of the ratio of the distance between the two light-scattering points and the distance from the second light-scattering point to the center of the ion trap. Therefore, the pulsed laser hits the particles when they arrive at the center of the trap regardless of the particle velocity or size.

The recorded count-up number was converted to a time-of-flight between the two light-scattering points by dividing the number of counts by the clock frequency. Since there was a direct correlation between particle time-of-flight and aerodynamic particle size (*21*), the size of each mass analyzed particle was determined from a calibration curve generated by measuring a set of known sized latex spheres. This system provided size and mass spectral information for each individually analyzed particle.

The ion trap was assembled from the quadrupole electrodes and electronics package from a Finnagan MAT ion trap mass spectrometer (*19*). The electrodes were housed in a 6 in. cubical chamber pumped with a 150 L/s turbomolecular pump. Holes of 3 mm diameter were drilled into the ring electrode to provide paths for the excimer laser and particle beams. Mass spectra of the ablated and trapped ions were obtained by ramping the rf voltage on the ring electrode of the trap (*22*). Positive ions were detected by a Channeltron multiplier through a hole on the end cap electrode. Negative ions may be detected with the same system indirectly by means of a conversion dynode near the Channeltron (*23*).

The mass scan electronics were synchronized to the ablation/ionization laser pulse in the following manner. The ion trap was operated in the "chromatograph" mode where the control circuitry makes and stores repeated scans. A typical scan consisted of an ion collection period, an ion selection period where all ions but those with the mass of interest were expelled from the trap, a collision induced dissociation (CID) period where the selected ions were excited at their secular frequency so that collisions with a bath gas cause fragmentation, followed by a mass scan of the product ions (*24*). The ionization gate signal was used to signal the start of the scan to our timing electronics. At this time, a TTL high was sent to halt the microprocessor controlling the ion trap. The trap then remained in ion collection mode until a particle was sampled. If a particle was detected at both PMTs within a given time window, then the excimer laser was fired. At this time, a TTL low was sent to the microprocessor to resume the scan function. The laser trigger was then disabled until a new scan was started. Primary mass spectra were obtained by eliminating the ion selection and CID periods in the scan function.

Samples were collected in a large polyethylene bag through a 1 in. I.D. hose directly from the diesel engine's exhaust pipe. The exhaust was sampled under three separate conditions: (1) just after the cold engine was started and idling at 1000 rpm, (2) after the engine had warmed to its

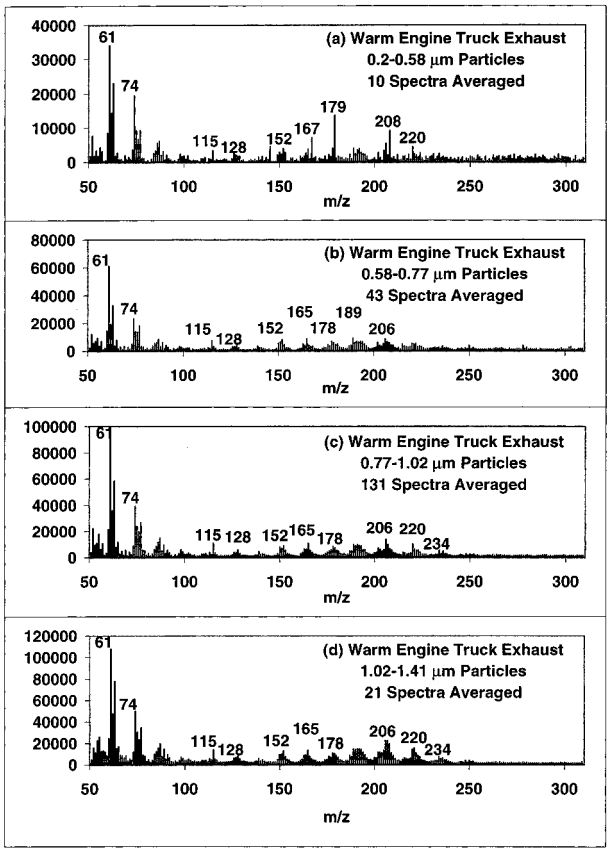

FIGURE 6. Individual exhaust particle mass spectra from a warm diesel engine idling at 1000 rpm averaged over a specified aerodynamic particle size range: (a) 0.2−0.58 μm range, 10 spectra averaged, (b) 0.58−0.77 μm range, 43 spectra averaged, (c) 0.77−1.02 μm range, 131 spectra averaged, (d) 1.02−1.41 μm range, 21 spectra averaged.

operating temperature while idling at 1000 rpm, and (3) with the warmed engine operated at 2000 rpm. The data were taken immediately following sample collection. A vented hose was connected between the sample bag and the particle inlet. The vent was used to dilute the exhaust particles with room air to reduce clogging of the inlet. One thousand particle mass spectra were taken in less than 10 min. All the exhaust particle data shown here were taken in less than a 2.5 h time span. This apparatus could readily be used for on-line analysis by merely connecting the vented hose directly to the exhaust particle source.

Results and Discussion

The purpose of this paper is to demonstrate the utility of the real-time aerosol ion trap technique for on-line measurements of particles containing organic species. While the measurements that we present are not truly performed on-line because the exhaust was first collected in a large plastic bag, they do represent real-time sampling of an aerosol. The only thing required to convert the measurements to on-line is to move the instrument close enough to connect the sampling hose to the inlet. No other modification is needed. On-line simultaneous measurement of particle size and organic composition of individual exhaust particles provides valuable insight into the combustion process as well as immediate diagnostics for engine performance and conditions.

The individual exhaust particle mass spectra taken under the above three conditions were averaged and are presented in Figure 2. Also presented in Figure 2 are averaged particle spectra from nebulized droplets of diesel fuel and motor oil. These averages were used as references for comparison with each other and their respective single particle mass spectra. The averaged mass spectra appear to consist of two distinct regions: a low-mass region from m/z 50 to 100 that contains sharp mass distributions consisting primarily of carbon clusters, (C_nH_m), and a high-mass region above m/z 100 whose local intensity distributions start out quite sharp at m/z 115 and rapidly broaden with increasing mass. All of the averaged spectra in Figure 2 were relatively similar in all cases except for the nebulized oil where there was much lower spectral intensity in the high-mass region and a significant change in the ion distribution in the low-mass region. Because of the similarity between the diesel fuel and exhaust spectra, one might assume the exhaust particles are composed of unburned diesel fuel. However, there was a difference between the diesel fuel spectra and the exhaust particle spectra at higher mass. Above approximately m/z 170, the peak distributions for the diesel fuel shifted toward higher mass relative to the exhaust. This shift indicates that on average the diesel fuel undergoes some degree of oxidation passing through the engine. Very little difference between the exhaust particle-averaged mass spectra from the warm engine running at 1000 and 2000 rpm was observed. However, there was a substantial increase in the ratio of relative intensities in the high-mass to low-mass regions of the spectra from the cold engine idling at 1000 rpm as compared to the spectra from the other engine conditions.

At first glance, the spectra in Figure 2 appear to be broadened by space charge effects. This was not the case here. In an ion trap, space charge manifests as a destabilization of the ions. As the rf is ramped, the ions that are destabilized due to space charge are expelled from the trap early resulting in broadening toward the low rf side of the ramp. When the excessive charge is bled off, normal stability conditions exist and the high rf side of the mass peak remains unbroadened. The broadening in Figure 2 was in fact a result of averaging because the actual distributions varied from particle to particle. The above points are illustrated in Figure 3, panels a and b. Figure 3a reveals the spectrum with the highest total ion count of all the individual particle spectra in any of the averages. If any of the spectra should show evidence of space charge, then it would be present here also. This spectrum clearly shows no evidence of peak broadening or space charge effects. It also represents one extreme in the variety of exhaust particle compositions where there was little intensity in the high-mass region of the spectrum. The other extreme can be observed in Figure 3b where there was little intensity in the low-mass region of the spectrum. The local peak distribution was noticeably broad, yet the relative integrated ion count was almost a factor of 3 lower than the spectrum in Figure 3a. This indicates that the local distribution about a peak maximum was due to varying degrees of hydrogenation. High- and low-mass extremes similar to those shown in Figure 3, panels a and b, were observed in all exhaust data sets. Between these extremes, the particle mass spectra have significant intensity in both the high- and low-mass regions. Moreover, all of the individual spectra of the exhaust particles may be loosely envisioned as linear combinations of the high- and low-mass extremes. Surprisingly, the same was true for the diesel fuel as well as the motor oil mass spectra; however, in these cases, the extremes have shifted mass distributions.

Figure 3c was included as a visual aid to help identify the masses below 170. This spectrum was from pine wood smoke (*25*) and represents a classic PAH mass distribution that one might observe in combustion particles. All of the peaks labeled in this spectrum were due to PAHs. Comparison reveals that the local peak distributions between m/z 77 and 170 in Figures 2 and 3b were most probably due to PAHs. (This will be confirmed later in this article by tandem mass

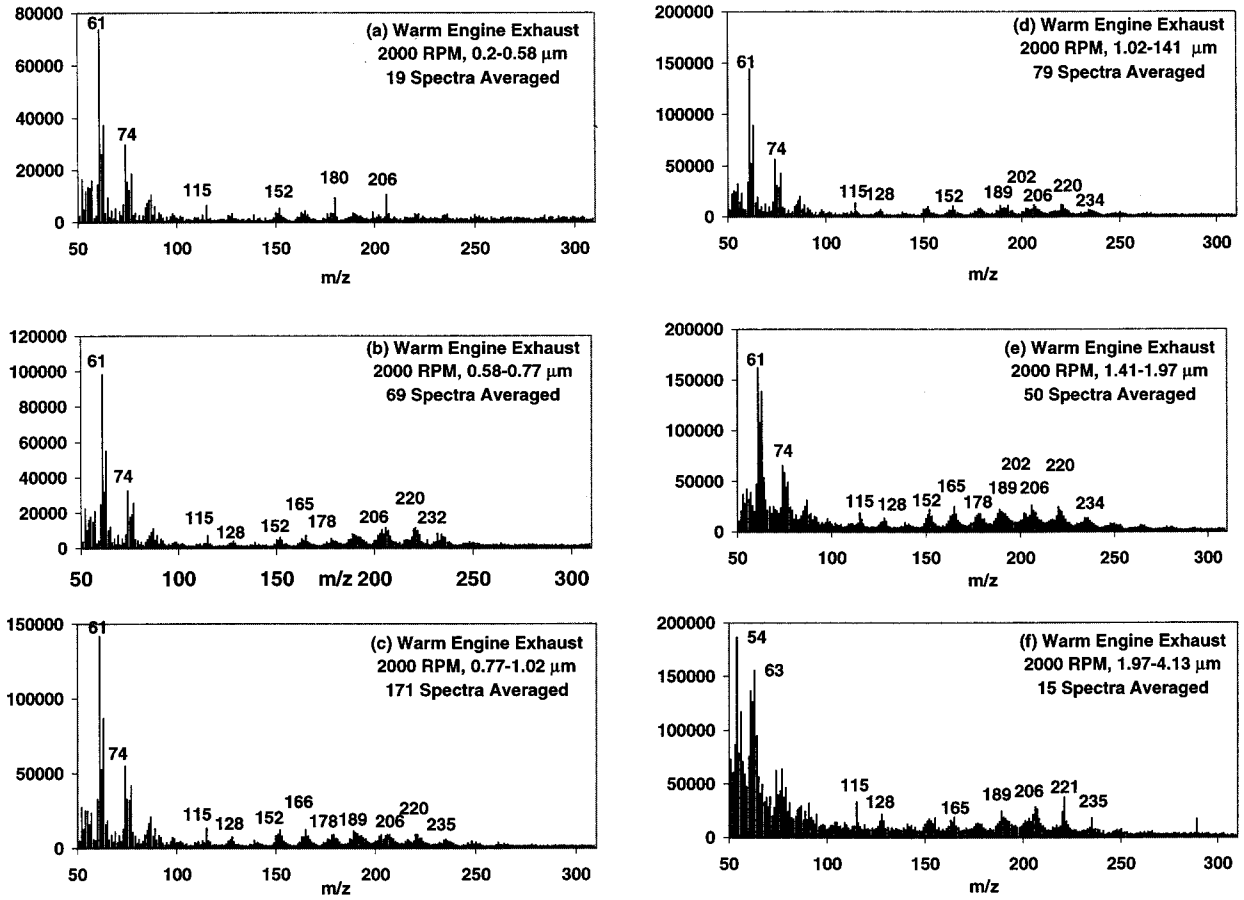

FIGURE 7. Individual exhaust particle mass spectra from a warm diesel engine running at 2000 rpm averaged over a specified aerodynamic particle size range: (a) 0.2−0.58 μm range, 19 spectra averaged, (b) 0.58−0.77 μm range, 69 spectra averaged, (c) 0.77−1.02 μm range, 171 spectra averaged, (d) 1.02−1.41 μm range, 79 spectra averaged, (e) 1.41−1.97 μm range, 50 spectra averaged, and (f) 1.97−4.13 μm range, 15 spectra averaged.

spectrometry.) Above m/z 170, the peak of the local mass distribution deviated from that for a PAH toward higher mass. The identification of these higher mass ions was not intuitively obvious and therefore required a higher order analytical technique such as MS/MS.

The measured aerodynamic particle size distributions of the exhaust particles whose mass spectra were used to create the averages shown in Figure 2 are presented in Figure 4. Collection of the exhaust in a bag before measurement may have a substantial effect on the measured particle size distribution. This is primarily due to the coalescence one would expect from the drop in temperature in going from the exhaust pipe to the bag environment. There should be much less affect on the particle composition because the chemical composition of the particle environment should not substantially change in going from the exhaust pipe to the bag. Since the exhaust was collected in a plastic bag before measurement, the measured distributions have not been corrected for size-dependent detection efficiency because the corrected distributions would not give an accurate representation of size dependent number density in the exhaust. However, this information could readily be obtained by direct measurement at the exhaust pipe with a portable version of our apparatus and the size-dependent detection efficiency curve for our apparatus (*18, 26*).

The size distribution from the cold engine exhaust was relatively broad and then narrowed considerably as the engine came to its thermal steady state as the truck idled. When the engine speed was increased to 2000 rpm (twice its idle speed), the peak of the distribution shifted to a slightly larger particle size and the distribution again broadened. There is a precipitous falloff in the size distribution below 0.5 μm that is due to inefficient transmission of particles through the inlet in this range. This falloff can be readily corrected using the previously mentioned size-dependent efficiency curve (*26*). The particle size detection limit of our apparatus is approximately 200 nm.

To see if there was a correlation between particle size and composition, the spectra were sorted as a function of particle size into six different bins. The spectra in each bin were then averaged. The results from the cold, warm and "high speed" engine conditions are presented in Figures 5, 6, and 7, respectively. The composition of the exhaust particles from the cold engine, Figure 5, shows a definite size dependence. As the particle size increased, the relative intensity of the lower mass peaks significantly decreased. It was not surprising that, for the warm engine at idle, there was no overt dependence of the exhaust particle composition on particle size (Figure 6), since the size distribution was dispersed over a rather narrow range. Although the size distributions of the exhaust particles from the cold engine at 1000 rpm and the warm engine at 2000 rpm are similar, compositional dependence on particle size for the warm 2000 rpm condition is more similar to the warm 1000 rpm condition (see Figure 7).

There is an increase in the number of low-mass range ions in going from a cold to a warm engine at idle. The ratio of relative intensities in the low- to the high-mass range could be used as a diagnostic for combustion efficiency, because warm engines are known to be more efficient than cold engines. Similarly, an increase in the size distribution without a corresponding change in size-dependent composition can

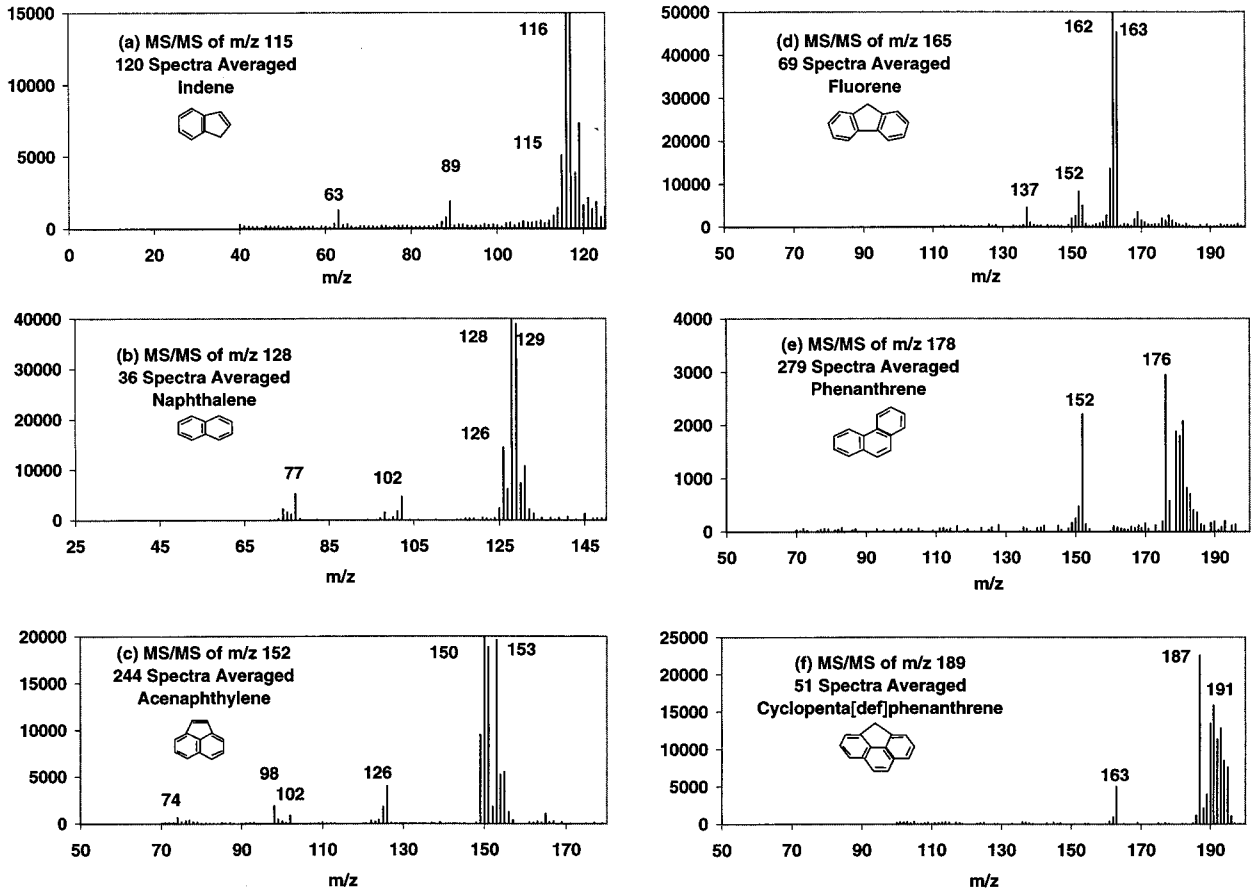

FIGURE 8. Averaged product ion spectra and proposed source structures: (a) MS/MS of *m/z* 115, indene, (b) MS/MS of *m/z* 128, naphthalene, (c) MS/MS of *m/z* 152, acenaphthylene, (d) MS/MS of *m/z* 165, fluorene, (e) MS/MS of *m/z* 178, phenanthrene, (f) MS/MS of *m/z* 189, cyclopenta[*def*]phenanthrene.

be used as a diagnostic for engines operating under load. With a portable version of this instrument, these measurements could be made in real-time while the vehicle is moving down the highway without the need for an expensive test facility.

The primary mass spectra only suggest that low molecular weight PAHs were detected in the exhaust particles, fuel, and oil and perhaps indicate the nature of the higher mass distribution. Tandem mass spectrometry provides confirmation of the identities of the low molecular weight PAHs and proposed structures for the higher mass ions. Figure 8 shows the MS/MS spectra of the low-mass PAHs under warm engine conditions. The listed masses were isolated using standard DC and rf techniques after laser ionization. An rf potential at the secular frequency of the isolated mass was then applied to the endcap electrodes to energize the isolated ions. Collisions with a helium bath gas at approximately 10^{-3} Torr caused the isolated ions to fragment during the excitation process. The masses were then scanned. The product ion spectra of the isolated ions are presented in each of the panels. The MS/MS spectra show ions with m/z greater than the precursor ion due to imperfect isolation. Since the precursor ions were resonantly energized, the higher mass ions did not fragment and did not contribute to the product ion spectrum. Also given is the name and structure of the compound whose electron impact ionization spectrum from the NIST/EPA/NIH Mass Spectral Database most closely resembles the product ion spectrum in terms of overall fragmentation pattern. (Quantitative comparison the relative intensities could not be performed due to the obvious differences in techniques). However, other viable structures could easily have given rise to the same product ion spectrum. For example, anthracene will yield essentially identical product ion mass spectra as those shown in Figure 8e. This is because PAHs generally undergo isomerization before fragmentation (*27*). Therefore, isomeric PAHs yield essentially the same mass spectra and probably do exist in the exhaust particle spectra. The structures presented here are, in general, the most likely based on thermodynamic considerations (*28*).

MS/MS was also performed on the ions above m/z 200 where the deviation from a PAH mass distribution is significant (see Figure 3, panels b and c). Figure 9 shows the product ion spectra of m/z 206, 208, 210, 220, and 222, respectively. The similarity of all of the spectra in this figure is quite noteworthy and hints at analogous structures. A very consistent fragmentation pattern is readily apparent in Figure 9, panels b, c, and e. These spectra consistently yield a pattern of smaller fragments at m/z 152, 165, and 178 and indicate a common PAH-like precursor structure. All of the spectra in Figure 9 yield manifolds of ions between m/z 189 and 195 and between m/z 202 and 207 regardless of the precursor mass. Losses of 4 and 5 hydrogen atoms from the precursors to yield m/z 202 and 203, respectively, in Figure 9 a and b, further support the suggestion of PAH-like precursor ions.

Since the precursor ions are produced from smoke, one would not expect to find a single compound to be the source of any of the precursor ions. However, one might expect to find a class of compounds that yield these types of MS/MS spectra. A search of the NIST/EPA/NIH Mass Spectral Database was again performed in terms of overall fragmentation pattern. The search was performed by mass and constrained to include only compounds containing carbon,

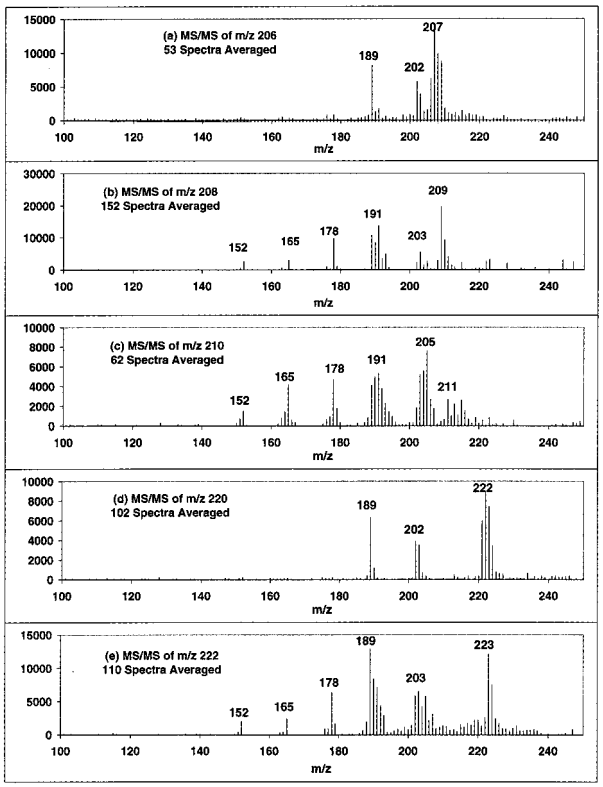

FIGURE 9. Averaged product ion spectra from: (a) *m/z* 206, (b) *m/z* 208, (c) *m/z* 210, (d) *m/z* 220, and (e) *m/z* 222.

hydrogen, nitrogen, and oxygen. Only hydrogenated PAHs (HPAHs) emerged as the likely source of the precursor ions. Methylated PAHs could account for some of the precursor masses in the mass spectrum. For example, dimethyl phenanthrene could account for the product ion spectrum from m/z 206, but it could not account for the product ion spectra from m/z 208 or 210 without hydrogenation. Moreover, no class of nitrogen- or oxygen-containing compounds yield spectra that would readily explain the fragment distribution of the product ions in the MS/MS spectra. However, this does not mean that those classes of compounds are not present in our exhaust particle sampling. It only means that the relative concentrations are small in comparison to hydrogenated and perhaps methylated PAHs or they were ionized with lower efficiency.

HPAHs have not been measured or discussed in previous studies of combustion particles (*1*−*4*). However, these studies were not performed in real-time. The time lag between collection and measurement permit the HPAHs to dehydrogenate to become their corresponding PAH. This is because hydrogenation of PAHs is reversible and, in general, occurs under equilibrium conditions (*29*). The hydrogenation reactivity of PAHs increases with the number of aromatic rings (*30*). This occurs because there is a relatively low activation barrier to hydrogenation that decreases with an increasing number of aromatic rings (*31*). These facts explain the presence of the onset for hydrogenation as a function of increasing m/z. Equilibrium conditions should prevail in the soot matrix as well. This means that the relative degree of hydrogenation of the PAHs in the soot matrix should primarily depend on the concentration of hydrogen in the matrix. When the soot particles are exposed to sunlight and air, the concentration of hydrogen in the matrix should be depleted by reaction with oxygen or effusion of H_2. Given the large surface area-to-volume ratio for the soot particles, hydrogen depletion should occur rapidly. Hence, the HPAHs have a relatively short lifetime in the soot matrix under ambient conditions. To observe the HPAHs from the exhaust particles, real-time methods are required.

HPAHs appear to be present in the diesel fuel as well, as seen in Figure 2d. It is not surprising that HPAHs are present in the fuel since catalytic hydroprocessing is an important part of large-scale petroleum refining (*29*). This suggests that the diesel fuel is the primary source of HPAHS in the exhaust spectra. Comparison of the averaged exhaust and fuel spectra shows a noticeable difference in the peak distributions in the high-mass range, indicating that the diesel fuel does not come through the combustion process without some degree of dehydrogenation and reactive addition of C_nH_m. Therefore, the average degree of hydrogenation could also be used as a diagnostic for combustion efficiency.

The utility of this instrument for on-line analysis of exhausts and smokestacks has been demonstrated. It provides real-time information on the size and composition of individual smoke particles that may be used as diagnostics for combustion processes. The added advantage of the ion trap MS/MS capabilities make it ideal for investigation of organic particles because of its ability to identify individual ions in the mass spectra.

Acknowledgments

This research was sponsored by the Office of Research and Development, U.S. Department of Energy, under Contract DE-AC05-96OR22464 with Oak Ridge National Laboratory managed by Lockheed Martin Energy Research Corp.

Literature Cited

(1) Rogge, W. F.; Hildemann, L. M.; Mazurek, M. A.; Cass, G. R.; Simonelt, B. R. T. *Environ. Sci. Technol.* **1993**, *27*, 636.
(2) Westerhol, R. N.; Alsberg, T. E.; Frommelin, Å. B.; Strandell, M. E.; Rannung, U.; Winquist, L.; Grigoriadis, V.; Egebäck, K. E. *Environ. Sci. Technol.* **1988**, *22*, 925.
(3) Westerhol, R. N.; Almén, J.; Li, H.; Rannung, J. U.; Egebäck, K. E.; Grägg, K. *Environ. Sci. Technol.* **1991**, *25*, 332.
(4) Lewis, A. C.; Askey, S. A.; Holden, K. M.; Bartle, K. D.; Pilling, M. J. *J. High Resol. Chromatogr.* **1997,** *20*, 109.
(5) Reed, G. A. *J. Environ. Sci. Health* **1988**, *C6*, 223.
(6) Pierce, R. C.; Kratz, M. *Environ. Sci. Technol.* **1975**, *9*, 347.
(7) Schwartz, J. *Environ. Res.* **1994,** *64*, 36.
(8) Dockery, D. W.; Schwartz, J.; Spengler, J. D. *Environ. Res.* **1992,** *59*, 362.
(9) Sinha, M. P. *Rev. Sci. Instrum.* **1984**, *55*, 886.
(10) McKeown, P. J.; Johnston, M. V.; Murphy, D. M. *Anal. Chem.* **1991**, *63*, 2069.
(11) Kievit, O.; Marijinissen, J. C. M.; Verheijen, P. J. T.; Scarlett, B. *J. Aerosol Sci.* **1992**, *23* (Suppl. 1), S301.
(12) Prather, K. A.; Nordmeyer, T,; Salt, K. *Anal. Chem.* **1994**, *66*, 1403.
(13) Hinz, K. P.; Kaufmann, R.; Spengler, B. *Anal. Chem.* **1994**, *66*, 2071.
(14) Murphy, D. M.; Thomson. D. S. *Aerosol Sci. Technol.* **1995**, *22*, 237.
(15) Carson, P. G.; Neubauer, K. R.; Wexler, A. S. *J. Aerosol Sci.* **1995**, *26*, 535.
(16) Reents, W. D., Jr.; Downey, S. W.; Emerson, A. B.; Mujsce, A. M.; Miller, A. J.; Siconolfi, D. J.; Sinclair, J. D.; Swanson, A. G. *Aerosol Sci. Technol.* **1995**, *23*, 263.
(17) Reilly, P. T. A.; Gieray, R. A.; Yang, M.; Whitten, W. B.; Ramsey, J. M. *Anal. Chem.* **1997**, *69*, 36.
(18) Gieray, R. A.; Reilly, P. T. A.; Yang, M.; Whitten, W. B.; Ramsey, J. M. *J. Microbiol. Methods* **1997**, *29*, 191.
(19) Yang, M.; Reilly, P. T. A.; Borass, K. B.; Whitten, W. B.; Ramsey, J. M. *Rapid Commun. Mass Spectrom.* **1996**, *10*, 347.
(20) Gieray, R. A.; Reilly, P. T. A.; Yang, M.; Whitten, W. B.; Ramsey, J. M. *Anal. Chem.* **1998**, *70*, 117.
(21) Noble, C. A.; Prather, K. A. *Environ. Sci. Technol.* **1996**, *30*, 2667.
(22) Stafford, G. C., Jr.; Kelley, P. E.; Syka, J. E. P.; Reynolds, W. E.; Todd, J. F. J. *Int. J. Mass Spectrom. Ion Processes* **1984**, *60*, 85.
(23) McLuckey, S. A.; Glish, G. L.; Kelley, P. E. *Anal. Chem.* **1987**, *59*, 1670.

(24) McLuckey, S. A.; Glish, G. L.; Van Berkel, G. J. *Int. J. Mass Spectrom. Ion Processes* **1991**, *106*, 197.
(25) Reilly, P. T. A.; Gieray, R. A.; Yang, M.; Whitten, W. B.; Ramsey, J. M. *Proc. 45th ASMS Conf.* **1997**, 202.
(26) Reilly, P. T. A.; Gieray, R. A.; Yang, M.; Whitten, W. B.; Ramsey, J. M. *Proc. 45th ASMS Conf.* **1997**, 466.
(27) Pachuta, S. J.; Kentt×**c2**maa, H. I.; Sack, T. M.; Cerny, R. L.; Tomer, K. B.; Gross, M. L.; Pachuta, R. R.; Cooks, R. G. *J. Am. Chem. Soc.* **1988**, *110*, 657.
(28) Stein, S. E.; Fahr, A. *J. Phys. Chem.* **1985**, *89*, 3714.
(29) Girgis, M. J.; Gates, B. C. *Ind. Eng. Chem. Res.* **1991**, *30*, 2021.
(30) Korre, S. C.; Klein, M. T.; Quann, R. J. *Ind. Eng. Chem. Res.* **1991**, *34*, 101.
(31) Sen, R.; Sumathy, R.; Rao, C. N. R. *THEOCHEM* **1996**, *361*, 211.

Received for review February 9, 1998. Revised manuscript received June 15, 1998. Accepted June 23, 1998.

ES980135T